CHARACTERIZATION OF REPRESENTATIVE VORTEX SURFACES IN K-TYPE TRANSITIONAL BOUNDARY LAYER

Yaomin Zhao

State Key Laboratory for Turbulence and Complex Systems
College of Engineering, Peking University
Beijing 100871, China
zym89@pku.edu.cn

Yue Yang

State Key Laboratory for Turbulence and Complex Systems
College of Engineering, Peking University
Beijing 100871, China
yyg@pku.edu.cn

Shiying Xiong

State Key Laboratory for Turbulence and Complex Systems
College of Engineering, Peking University
Beijing 100871, China
syxiong@pku.edu.cn

Shiyi Chen

State Key Laboratory for Turbulence and Complex Systems
College of Engineering, Peking University
Beijing 100871, China
syc@pku.edu.cn

ABSTRACT

We apply the vortex-surface field (VSF), a Lagrangian-based structure-identification method, to the DNS database of the K-type transitional boundary layer (Sayadi *et al.*, 2013). The VSFs are constructed from the vorticity fields within a sliding window at different times and streamwise locations using a recently developed boundary-constraint method. The isosurfaces of the VSF, representing vortex surfaces consisting of vortex lines with different wall distances in the laminar stage, show different evolutionary geometries in the transition. We observe that the vortex surfaces evolve from wall-parallel planar sheets through hairpin-like structures into a turbulent spot with offspring hairpins. From quantitative analysis, we show that a small number of representative vortex surfaces can contribute significantly to the increase of the skin-friction coefficient in the transition, which implies a reduced-order model based on the VSF.

INTRODUCTION

Transitional wall flows are statistically non-equilibrium and are characterized by the emergence of coherent structures evolving from large-scale simple structures into multi-scale complex structures. Although the role played by the coherent structures is still not fully understood, many studies have provided evidence supporting the hypothesis that these structures are important for drag reduction and turbulence control in transitional wall flows (Robinson, 1991; Adrian, 2007). Our aim is to elucidate the late transition by characterizing the dynamical evolution of a small number of representative vortical structures.

The vortex-surface field (VSF), a Lagrangian-based structure identification method, is developed to study the evolution of vortical structures in viscous flows (Yang & Pullin, 2010, 2011). This method is rooted in the Helmholtz vorticity theorem for inviscid flows, and introduces a two-time approach and a numerical dissipative regularization for viscous flows. Every iso-surface of the VSF ϕ_v that is a three-dimensional globally smooth scalar defines a vortex surface consisting of vortex lines. A systematic methodology is developed for constructing smooth VSFs in simple laminar flows (Yang & Pullin, 2010; Zhao *et al.*, 2016*a*), and then the equations describing the evolution of VSFs are obtained (Yang & Pullin, 2011).

The VSF method has been successfully applied to viscous highly symmetric flows (Yang & Pullin, 2011) and transitional channel flows (Zhao *et al.*, 2016*b*). The evolution of VSFs suggests a possible scenario for explaining vortex dynamics in the laminar-turbulent transition and scale cascade in terms of topology and geometry of vortex surfaces. In order to characterize the continuous vortex dynamics, the VSF uses evolving vortex surfaces along with

attached vortex lines and their vorticity magnitude, which combines the strengths of existing identification methods used in wall turbulence. As a natural extension, it is interesting to apply the VSF to the transitional boundary layer.

Owing to the lack of a universal transition mechanism, the transitional wall flow is also a challenging paradigm for developing simple predictive models. For example, although the large-eddy simulation (LES) can resolve the unsteady large-scale motion, Sayadi & Moin (2012) found that most of the subgrid scale (SGS) models in LES significantly underpredict the skin friction in transitional boundary layers on coarse grids, particularly for the late nonlinear stage. The existing SGS models fail to provide the accurate contribution of SGS motions to large-scale motions in the near-wall region where small-scale, anisotropic coherent structures are important in inducing the scale cascade in the transition. In addition, the wall-resolved LES is hard to be used in high-Reynolds-number wall flows due to its high computational cost.

Instead of resolving the near-wall structures, the wall-modeled LES (WMLES) uses a reduced-order model to simplify the under-resolved near-wall flow as a modified boundary condition (Park & Moin, 2014). Since the existing wall models are developed only for fully developed turbulent flows, the transitional flow is still challenging for WMLES. In implementations, an ad hoc sensor is required to artificially switch off the wall model in the laminar region. Hence, we need improved reduced-order models for transitional wall flows with evolutionary coherent structures.

Furthermore, some decomposition methods, e.g., the proper orthogonal decomposition (Berkooz *et al.*, 1993), the dynamic mode decomposition (DMD) (Schmid, 2010), and the resolvent-mode decomposition (Mckeon & Sharma, 2010), have been developed to characterize near-wall coherent structures using a small number of modes. In particular, the DMD has been applied to transitional boundary layers to assess the contribution of coherent structures to flow statistics (Sayadi *et al.*, 2014), and *a priori* tests show that several low-frequency DMD modes can provide an accurate estimate of the skin-friction coefficient in the transition. These reduced-order representations appear to be useful in improving our understanding of the dynamics of coherent structure, though they have yet to be predictive models in *a posteriori* tests for transitional wall flows.

In the present study, the VSF is applied to the DNS database of the Klebanoff-type (K-type) transitional boundary layer reported in Sayadi *et al.* (2013). Statistical study based on the VSF is then used to analyze the contribution of a set of representative vortex surfaces to the flow statistics. The characterization of a small number of representative vortex surfaces may shed light on a structure-based decomposition and a reduced-order presentation.

Moreover, two recently developed techniques are used, including the boundary-constrained method (Xiong & Yang, 2017) for constructing VSFs, and the sliding window filter (Zheng *et al.*, 2016) for extracting spatially developed coherent structures. These two methods can alleviate the high computational cost for calculating VSFs.

CONSTRUCTION OF VSF
The boundary-constraint method

Given a three-dimensional vorticity field $\omega(x,t)$ at a time instant t, the VSF ϕ_v is defined to satisfy the constraint (Yang & Pullin, 2010)

$$\mathscr{C}_v \equiv \omega \cdot \nabla \phi_v = 0, \qquad (1)$$

so that every isosurface of ϕ_v is a vortex surface consisting of vortex lines. The evolution of the VSF can be calculated using the

two-time approach (Yang & Pullin, 2011), but it requires a temporally resolved series of velocity fields with the nearly zero-helicity-density initial field, and its computational cost can be much higher than that of the DNS for velocity fields.

Recently, Xiong & Yang (2017) developed a new boundary-constraint method for constructing VSFs. It needs only a single velocity field to calculate the VSF at a given time instead of using a time series of DNS velocity database in the two-time approach. The boundary-constraint method requires that most of the vortex lines in the given velocity field should pass through boundaries, so it can be used for shear flows. In addition, the VSFs constructed from the velocity fields at different times in the K-type transition are shown to be consistent with the results from the two-time approach.

The basic idea of the boundary-constraint method is illustrated in Figure 1. We impose the VSF constraint $\mathscr{C}_v$ at the lateral boundary and advect the constraint into the entire domain Ω using the frozen vorticity field as

$$\frac{\partial \phi_v(x,t;\tau)}{\partial \tau} + \omega(x,t) \cdot \nabla \phi_v(x,t;\tau) = 0, \quad x \in \Omega, \ \tau > 0, \quad (2)$$

$$\omega(x,t) \cdot \nabla \phi_v(x,t;\tau) = 0, \quad x \in \partial\Omega, \ \tau > 0, \quad (3)$$

$$\phi_v(x,t;\tau) = \phi_0(x,t), \quad x \in \Omega, \ \tau = 0, \quad (4)$$

where $\phi_0(x,t)$ is a given initial condition, and τ is pseudo-time. In Eq. (2), ϕ_v is transported by the frozen vorticity $\omega(x,t)$. The corresponding transport equation for $\mathscr{C}_v$ has the same form as Eq. (2) with $\mathscr{C}_v = 0$ at boundaries. Thus, $\phi_v(x,t;\tau)$ can converge to the desired VSF through the evolution in pseudo-time as

$$\phi_v(x,t) = \lim_{\tau \to \infty} \phi_v(x,t;\tau). \qquad (5)$$

The maximum pseudo-time T_τ depends on the given error tolerance. In the present implementation, the deviation $\lambda_\omega = \omega \cdot \nabla \phi_v / (|\omega||\nabla \phi_v|)$ is controlled below 5% and the corresponding T_τ is 0.26 with $O(10^5)$ pseudo-time steps.

Eq. (2) is advanced in τ using the third-order total-variation-diminishing Runge-Kutta method, and the convection term is treated by the fifth-order weighted essentially nonoscillatory (WENO) scheme (Jiang & Shu, 1996). The numerical diffusion in the WENO scheme can serve as a numerical dissipative regularization for Eq. (2). Moreover, in order to increase the computational accuracy and efficiency in the calculation of Eq. (2), two ghost zones are added next to the lateral boundaries of the computation domain. In the ghost zones, vortex lines are artificially stretched to be normal to the leftmost or the rightmost boundary, as illustrated in Figure 1. More details of the boundary-constraint method can be found in Xiong & Yang (2017).

Construction of VSFs in the transitional boundary layer

The boundary-constraint method is applied to the DNS database of the K-type boundary-layer transition (Sayadi *et al.*, 2013) at the Center for Turbulence Research (CTR) at Stanford University. In the DNS, the fully compressible Navier-Stokes equations are solved with the fourth-order finite difference scheme. The Mach number $Ma = 0.2$ is sufficiently low for compressibility effects to be negligible. The inlet Reynolds number based on the distance from the leading edge and the free-stream velocity is $Re_x = 10^5$, and the distance of the inlet station from the leading edge of the plate x_0 is used as the reference length scale. Some parameters of the DNS are shown in Table 1, where N_x, N_y and N_z are the numbers
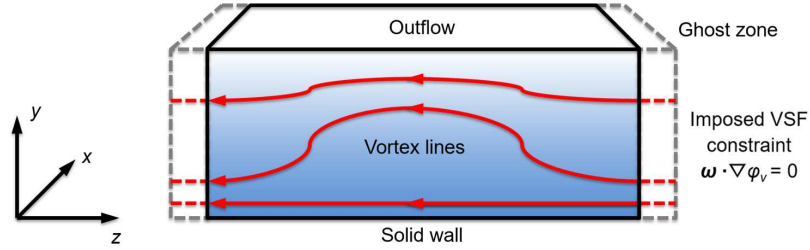
Figure 1. A schematic diagram of the boundary-constraint method for constructing the VSF in a transitional boundary layer (Xiong & Yang, 2017).

Cases	N_x	N_y	N_z	L_x	L_y	L_z	x_c
DNS	4096	550	512	8.6	0.92	0.6	5.30
W1	768	768	768	0.17	0.058	0.15	2.40
W2	768	768	768	0.25	0.058	0.15	2.71
W3	768	768	768	0.36	0.058	0.15	2.82
W4	768	768	768	0.42	0.058	0.15	3.09
W5	768	768	768	0.50	0.058	0.15	3.18

Table 1. Parameters of the DNS (Sayadi *et al.*, 2013) and the VSF calculations in different windows (W1–W5).

of grids in the streamwise, wall-normal and spanwise directions, respectively, and L_x, L_y and L_z are the sizes of the simulation domain non-dimensionalized by x_0. The Tollmien–Schlichting (TS) waves and the oblique waves are introduced within a narrow disturbance strip near the inlet. The width of the disturbance strip is $l_0 = 0.2$ and the spanwise wavelength of the oblique wave is $\lambda_0 = 0.15$. The computational domain used in the DNS contains $4\lambda_0$ in the spanwise direction.

As illustrated in Figure 2, the computational domain for the VSF calculations is extracted by a sliding window from the entire DNS domain. The parameters of the VSF computation are also shown in Table 1, where L_x, L_y and L_z are the sizes of the window, and x_c is the center of the sliding window in the streamwise direction. The sliding window with increasing x_c moves and stretches in the streamwise direction during the transition to capture the major deformation of the vortex surface whose streamwise extent in the laminar stage is l_0. Furthermore, the height of the sliding window is selected as $L_y = 0.058$, which is about $1 \sim 2$ boundary-layer thickness so that the nearly laminar field in the outer layer is excluded.

Moreover, as suggested in Zhao *et al.* (2016a), the initial VSF in Eq. (4) is set as $\phi_{v0} = y/L_y$. This initial condition ensures that the VSF is invariant in the mean shear flow and is compatible with the boundary conditions. We remark that the isosurfaces of ϕ_{v0} with $0 \leq \phi_{v0} \leq 1$ are stream surfaces at the initial time, and the contour level of ϕ_v denotes the wall distance of the wall-parallel vortex surfaces in the laminar stage.

Vortex surfaces with the same initial planar geometry and different initial wall-distances can have different evolutionary geometries in their evolution (Zhao *et al.*, 2016a). Those vortex surfaces that are very close to the wall or remote from the wall have only slight deformation owing to the relatively small disturbances in both regions. On the other hand, the vortex surfaces from the near-wall region can evolve into complex shapes, and they can be used to characterize the vortical structures in late transition. As sketched in Figure 2, these vortex surfaces evolve along with the rise of the skin-friction coefficient, which motivates the quantitative investigation of such representative vortex surfaces and their role in the local

increase in skin friction.

EVOLUTION OF VSF
Visualization on the evolution of VSFs

We consider isosurfaces of the VSF to study the evolution of vortex surfaces in the K-type transitional boundary layer. In Figure 3, the VSF isosurfaces of $\phi_v = 0.28$ at four different windows and times display signature vortical structures in the late transition. We define t_0 as the time for the first window in Figure 3(a), and the time interval between the snapshots are non-dimensionalized by the length scale x_0 and the free-stream sound speed. The vortex lines integrated from the isosurfaces are almost attached on the surfaces, which demonstrates the accuracy of the VSF calculation.

From the initial vortex surface parallel to the wall, the vortex surface first forms a triangular bulge in Figure 3(a), and then evolves into a series of hairpin-like structures in Figures 3(b) and (c). Under the effects of the mean-flow shear and the self-induced motion of the vortical structures, the hairpin-like structures are stretched and detached from the original bulge after their formation. Subsequently, the vortex surfaces under the hairpin heads are rapidly distorted, and the distortion propagates in the spanwise direction in a wave-like pattern in Figure 3(d), which can generate small-scale offspring hairpins. The regeneration of hairpins appears to trigger the formation of the turbulent spot and final breakdown into turbulence (Brinkerhoff & Yaras, 2014). We remark that the continuous evolution of vortical structures from a simple planar vortex surface through hairpin and structure packets to turbulent spot is visualized using the VSF isosurfaces with a single contour level representing the initial wall distance, rather than using different iso-contour levels as in most existing vortex identification methods.

In Figure 4, we compare the structures identified by the isosurface of the VSF, vortex lines and the isosurface of the Q-criterion (Hunt *et al.*, 1988). The structures identified by the vortex surface in Figure 4(a) show the regeneration of small-scale bulges and hairpins in the spanwise direction, and their Lagrangian-like evolution process can be deduced from the VSF isosurfaces in the sequential snapshots in Figure 3. In Figure 4(b), the vortex lines look chaotic and less coherent than the vortex surface in Figure 4(a), though they are integrated based on the VSF isosurfaces. In Figure 4(c), the Eulerian Q-criterion can identify the vortex cores, which coincide with the tube-like region with high curvature on the VSF isosurface. However, the Q-isosurface shows the visual "breakdown" of vortical structures, which cannot elucidate the vortex dynamics such as rolling up and reconnection. In general, the VSF method can combine the strengths of existing identification methods used in wall turbulence as well as revealing the Lagrangian vortex dynamics, and additional quantitative analysis can be obtained based on the VSF level sets.
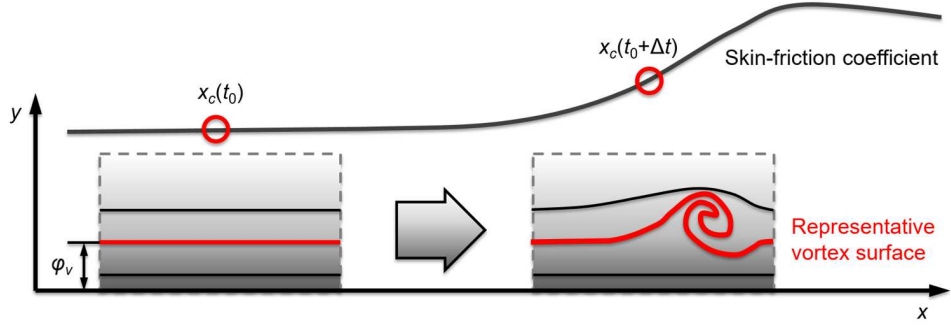
Figure 2. A schematic diagram of the rise of the skin-friction coefficient and the evolution of vortex surfaces in the transitional boundary layer. The representative vortex surface with significant deformation is shown by the thick solid line.
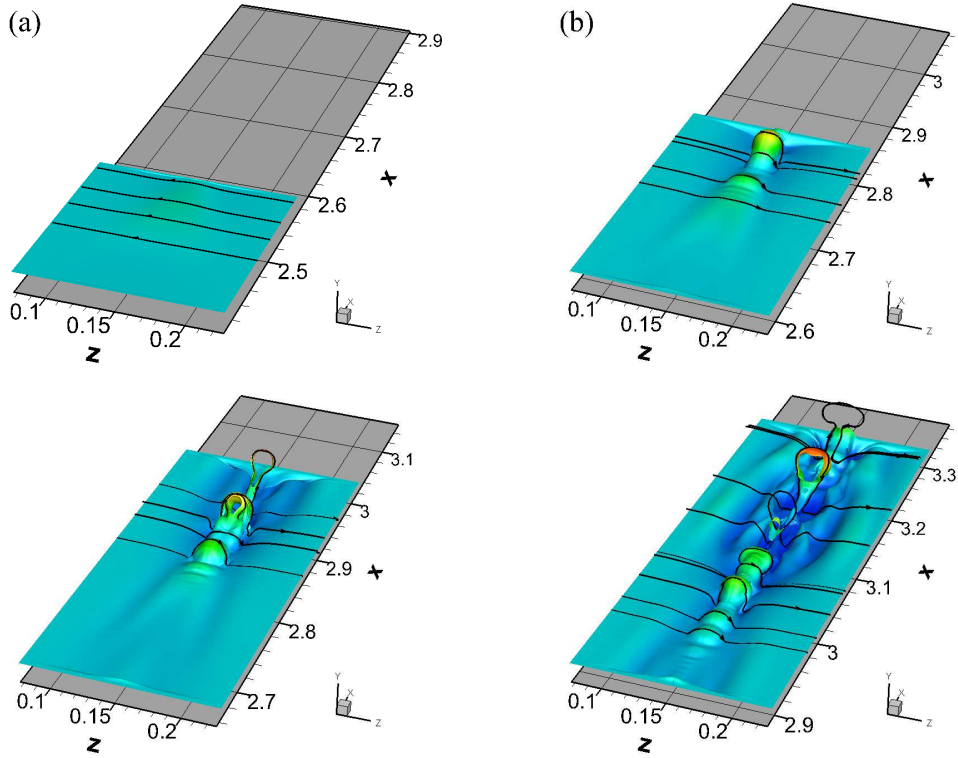

Figure 3. Evolution of the vortex surface of $\phi_v = 0.28$ in the K-type transitional boundary layer, (a) $x_c = 2.40$ and $t = t_0$; (b) $x_c = 2.71$ and $t = t_0 + 0.037$; (c) $x_c = 2.82$ and $t = t_0 + 0.055$; (d) $x_c = 3.09$ and $t = t_0 + 0.083$. The VSF isosurfaces are color-coded by y, and vortex lines are integrated from the surfaces.

Characterization of representative vortex surfaces

We have shown that the vortex surfaces with large deformation display signature vortical structures in the late stages of transition. These representative vortex surfaces may also be important in the dynamics of the transition process. In particular, we examine the relation between the representative vortex surfaces and the increase of the wall-friction in transition.

As derived by Fukagata *et al.* (2002), the wall-friction of plane boundary layers can be decomposed into different parts. One of the major part, the turbulent friction, can be written as

$$C_f^T = \int_0^\delta \langle (1 - \frac{y}{\delta})(-u'v') \rangle dy. \tag{6}$$

Here, the wall-friction coefficient $C_f \equiv 2\tau_w/(\rho U_\infty^2)$, and the wall-

shear stress is $\tau_w \equiv \rho \nu (\partial \langle u \rangle_z / \partial y)|_{y=0}$. Therefore, the increase of the wall-friction caused by turbulent fluctuations C_f^T can be represented by the weighted integral of the Reynolds shear stress.

To investigate the relations between the deformation of the vortex surfaces and the momentum transport in the transition, we present the contour of $-(1 - y/\delta)(u'v')$ on the spanwise symmetric plane at $z = L_z/2$ and $x_c = 2.71$ in Figure 5, along with VSF isolines $\phi_v = 0.1$ and $\phi_v = 0.2$. We can see that $-(1 - y/\delta)(u'v')$ concentrates in ribbon-like local regions, and the distribution appears to coincide with the hairpin-like structures enclosed by the VSF isolines, because the hairpins induce "ejections" and "sweeps" (Adrian, 2007) with large spatial variations of $u'v'$.

Based on the identification of the space-filling vortex surfaces, we quantify the contributions from different vortex surfaces with initial wall distances $0 \le \phi_v \le 1$ to the Reynolds shear stress and to
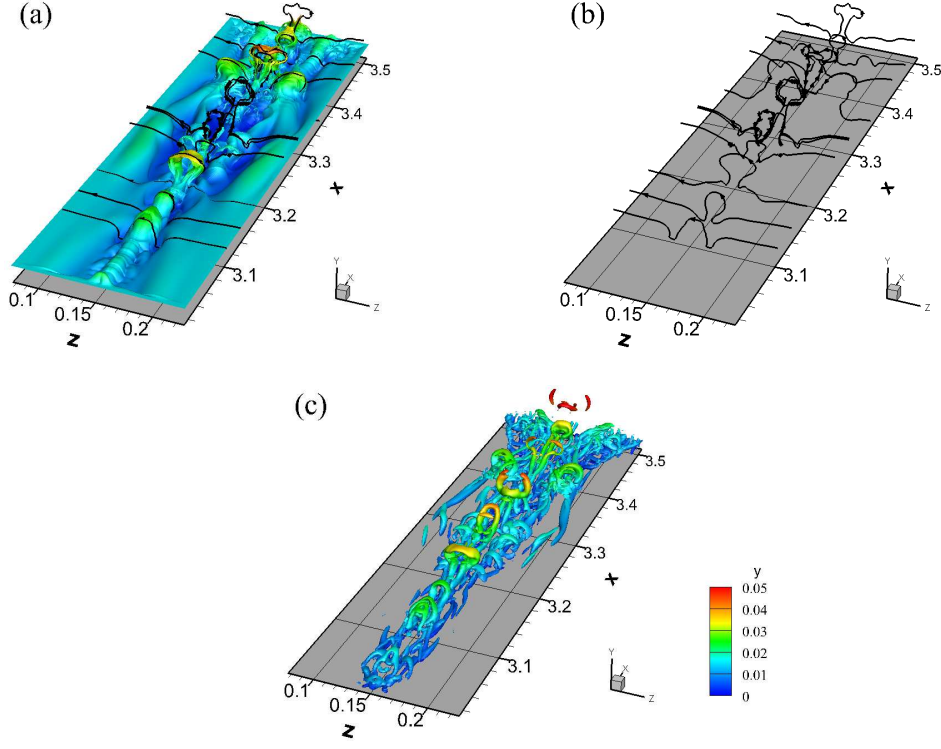
Figure 4. Vortical structures identified by different methods in the K-type transitional boundary layer at $x_c = 3.26$ and $t = t_0 + 0.101$, (a) VSF isosurface; (b) vortex lines; (c) Q-isosurface.
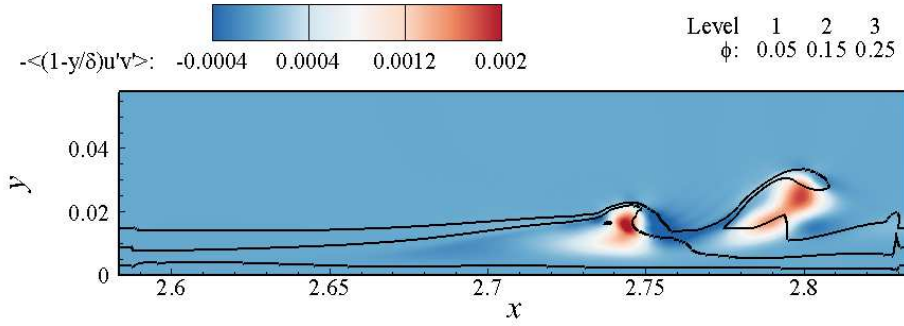

Figure 5. Contour of $-\partial(u'v')/\partial y$ and VSF isolines on the symmetric spanwise plane at $z = L_z/2$ and $x_c = 2.71$.

the skin friction. For an arbitrary function $f(x,y,z)$ at a particular y, we define the plane average as

$$\langle f \rangle \equiv \int_0^{L_x} \int_0^{L_z} f \, dx \, dz / A_{xz}, \qquad (7)$$

where $A_{xz} = \int_0^{L_x} \int_0^{L_z} dx \, dz$ is the plane area, and we define the VSF-based conditional average as $\langle f | \phi_1 \leq \phi_v \leq \phi_2 \rangle \equiv \int \int_{S_v} f \, dx \, dz / A_{xz}$, where S_v is the region with $\phi_1 \leq \phi_v \leq \phi_2$ on an x–z plane. Then $\langle -(1-y/\delta)(u'v') \rangle$ represents the weighted Reynolds shear stress averaged within the sliding window, and $\langle -(1-y/\delta)(u'v') | \phi_1 \leq \phi_v \leq \phi_2 \rangle$ denotes the contribution from the vortex surfaces with $\phi_1 \leq \phi_v \leq \phi_2$ to the weighted Reynolds shear stress. As shown in Figure 6, the vortex surfaces with $0.05 \leq \phi_v \leq 0.25$, which only occupy approximately 20% volume of the sliding window, can qualitatively capture the distribution of the weighted Reynolds shear stress. By integrating the weighted Reynolds shear stress as $\int_0^{L_y} |\langle -(1-y/\delta)(u'v') \rangle| \, dy$, we find that only 10%

and 20% of all the vortex surfaces contribute 43% and 70% of the skin-friction coefficient, respectively. This implies that the most of the contribution to drag production is from a small number of representative vortex surfaces. Therefore, the vortex surfaces with large deformation are also important in the transition dynamics, which suggests a reduced-order model based on the representative vortex surfaces.

CONCLUSION

The VSF, a Lagrangian-based structure identification method, is applied to the CTR DNS database of the K-type transitional boundary layer. In order to reduce the computation cost, the recently developed boundary-constraint method is used to construct the VSF. In the present study, we apply a sliding window to extract vorticity fields at different times and locations, and then the VSF pseudo-transport equation is solved based on the extracted vorticity fields in different windows.

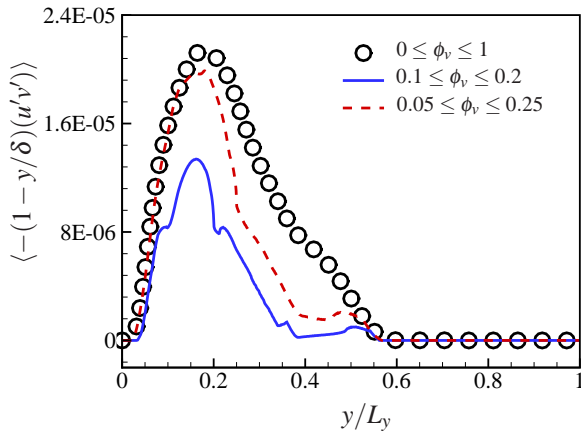Isosurfaces of the VSF are extracted to visualize the evolu-

Figure 6.   Reynolds shear stresses conditioned on different sets of vortex surfaces in the sliding window at $x_c = 2.71$.

tion of vortical structures. The VSF isosurfaces represent vortex surfaces consisting of vortex lines with different wall distances in the laminar state, and they show different evolutionary geometries in transition. We observe that the representative vortex surface evolves from a wall-parallel planar vortex surface through hairpin-like structures into a turbulent spot with the regeneration of small-scale hairpins in both streamwise and spanwise directions.

Furthermore, we quantitatively analyze the contribution of different vortex surfaces to the rise of the skin-friction coefficient in transition. The strong turbulent fluctuations generated by the hairpin-like structures concentrate in ribbon-like local regions, which are also packed by the vortex surfaces initially near the wall. The statistics conditioned on a small fraction of vortex surfaces can capture the distribution of the Reynolds shear stress, which implies that a small number of representative vortex surfaces can contribute significantly to the drag generation in the transition.

In future work, we aim to develop a formal framework to characterize the representative vortex surfaces and a reduced-order representation with a decomposition based on the VSF. In addition, the VSF method can be applied to the H-type (Sayadi *et al.*, 2013) and the bypass (Wu & Moin, 2010) boundary-layer transitions.

REFERENCES

Adrian, R. J. 2007 Hairpin vortex organization in wall turbulence. *Phys. Fluids* **19**, 041301.

Berkooz, G., Holmes, P. & Lumley, J. L. 1993 The proper orthogonal decomposition in the analysis of turbulent flows. *Annu. Rev. Fluid Mech.* **25**, 539–575.

Brinkerhoff, J. R. & Yaras, M. 2014 Numerical investigation of the generation and growth of coherent flow structures in a triggered turbulent spot. *J. Fluid Mech.* **759**, 257–294.

Fukagata, K., Iwamoto, K. & Kasagi, N. 2002 Contribution of reynolds stress distribution to the skin friction in wall-bounded flows. *Phys. Fluids* **14**, L73–76.

Hunt, J. C. R., Wray, A. A. & Moin, P. 1988 Eddies, stream, and convergence zones in turbulent flows. In *Proceedings of the Summer Program*, pp. 193–208. Center for Turbulence Research, Stanford University.

Jiang, G. S. & Shu, C. W. 1996 Efficient implementation of weighted ENO schemes. *J. Comput. Phys.* **126**, 202–228.

Mckeon, B. J. & Sharma, A. S. 2010 A critical-layer framework for turbulent pipe flow. *J. Fluid Mech.* **658**, 336–382.

Park, G. I. & Moin, P. 2014 An improved dynamic non-equilibrium wall-model for large eddy simulation. *Phys. Fluids* **24**, 015108.

Robinson, S. K. 1991 Coherent motions in the turbulent boundary layer. *Annu. Rev. Fluid Mech.* **23**, 601–639.

Sayadi, T., Hamman, C. W. & Moin, P. 2013 Direct numerical simulation of complete H-type and K-type transitions with implications for the dynamics of turbulent boundary layers. *J. Fluid Mech.* **724**, 480–509.

Sayadi, T. & Moin, P. 2012 Large eddy simulation of controlled transition to turbulence. *Phys. Fluids* **24**, 114103.

Sayadi, T., Schmid, P. J., Nichols, J. W. & Moin, P. 2014 Reduced-order representation of near-wall structures in the late transitional boundary layer. *J. Fluid Mech.* **748**, 278–301.

Schmid, P. J. 2010 Dynamic mode decomposition of numerical and experimental data. *J. Fluid Mech.* **656**, 5–28.

Wu, X. & Moin, P. 2010 Transitional and turbulent boundary layer with heat transfer. *Phys. Fluids* **22**, 085105.

Xiong, S. & Yang, Y. 2017 The boundary-constraint method for constructing vortex-surface fields. *J. Comput. Phys.* **339**, 31–45.

Yang, Y. & Pullin, D. I. 2010 On Lagrangian and vortex-surface fields for flows with Taylor–Green and Kida–Pelz initial conditions. *J. Fluid Mech.* **661**, 446–481.

Yang, Y. & Pullin, D. I. 2011 Evolution of vortex-surface fields in viscous Taylor-Green and Kida-Pelz flows. *J. Fluid Mech.* **685**, 146–164.

Zhao, Y., Yang, Y. & Chen, S. 2016a Evolution of material surfaces in the temporal transition in channel flow. *J. Fluid Mech.* **793**, 840–876.

Zhao, Y., Yang, Y. & Chen, S. 2016b Vortex reconnection in the late transition in channel flow. *J. Fluid Mech.* **802**, R4.

Zheng, W., Yang, Y. & Chen, S. 2016 Evolutionary geometry of Lagrangian structures in a transitional boundary layer. *Phys. Fluids* **28**, 035110.